



Shock wave-pretreated ADMSCs of cell-sheet scaffold (CSS) patched on the left ventricular wall (LVW) inhibited LVW remodeling in mini-pig MI: role of CSS on counteracting Laplace's Law of LVW stress – experimental study

Jiunn-Jye Sheu, MD^{a,b,c}, Jui-Ning Yeh, MD^d, Yin-Chia Chen, MD^a, John Y. Chiang, PhD^{e,f}, Pei-Hsun Sung, MD^{b,c,g}, Chi-Ruei Huang, PhD^{b,g}, Yi-Chen Li, PhD^g, Hon-Kan Yip, MD^{b,c,g,h,i,*}

Background: We investigated whether shock wave (SW)-pretreated autologous adipocyte-derived mesenchymal stem cells (ADMSCs) seeded in the cell-sheet scaffold (CSS) could inhibit left ventricular (LV) remodeling and improve LV ejection fraction (LVEF) in old myocardial infarction (MI).

Methods: Mini-pigs (n = 20) were divided into group 1 (sham-operated control), group 2 (old MI), group 3 (old MI + autologous ADMSCs/1.0×10⁷ in CSS on LV myocardium), and group 4 [old MI + SW (0.12 mJ/mm² for total 140 shots)-pretreated ADMSCs in CSS on LV myocardium]. Treatments started on day 28 after MI induction. In-vivo and in-vitro studies were conducted.

Results: Cell viability/relative mitochondria DNA expression/mitochondrial cytochrome C/adenosine triphosphate concentration in ADMCSs and protein expressions of angiogenesis factors [vascular endothelial growth factor (VEGF)/stromal cell-derived factor-1 (SDF-1)/mitochondrial respiratory chain complexes I–IV/oxygen consumption rate] were higher in group 4 than in group 3 (P < 0.001). By day 180, LVEF and small vessel numbers in the peri-infarct or infarct area were highest in group 1, lowest in group 2, and significantly lower in group 3 than in group 4. In contrast, the LV dimension was opposite to the pattern of change in LVEF in all groups (P < 0.0001). The basal/middle/apical infarct and fibrotic areas were inversely related to LVEF in all groups (all P < 0.0001). Protein levels of angiogenetic markers (SDF-1 α /C-X-C chemokine receptor type 4/VEGF/angiopoietin-1) were significantly and persistently increased from groups 1 to 4. In contrast, protein levels of endothelial cell markers (von Willebrand factor or endothelial nitric oxide synthase) showed an identical pattern to LVEF in all groups (all P < 0.0001).

Conclusion: SW pretreatment of ADMSCs seeded in CSS offered significant benefits in preserving LV performance and ameliorating LV remodeling in mini-pigs with old MI.

Keywords: angiogenesis, cell-sheet scaffold, extracorporeal shock wave, mesenchymal stem cells, old myocardial infarction

^aDivision of Thoracic and Cardiovascular Surgery, Department of Surgery, Kaohsiung Chang Gung Memorial Hospital and Chang Gung University College of Medicine, Kaohsiung, Taiwan, ROC, ^bCenter for Shockwave Medicine and Tissue Engineering, Kaohsiung Chang Gung Memorial Hospital, Kaohsiung, Taiwan, ROC, ^cInstitute for Translational Research in Biomedicine, Kaohsiung Chang Gung Memorial Hospital Kaohsiung, Taiwan, ROC, ^dDepartment of Cardiology, The First Affiliated Hospital, Jinan University, Guangzhou, China, ^eDepartment of Computer Science and Engineering, National Sun Yat-Sen University, Kaohsiung, Taiwan, ROC, ^fDepartment of Healthcare Administration and Medical Informatics, Kaohsiung Medical University, Kaohsiung, Taiwan, ROC, ^gDivision of Cardiology, Department of Internal Medicine, Kaohsiung Gung Memorial Hospital and Chang Gung University College of Medicine, Kaohsiung, Taiwan, ROC, ^hDepartment of Medical Research, China Medical University Hospital, China Medical University, Taichung, Taiwan, ROC and ^fSchool of Medicine, College of Medicine, Chang Gung University, Taoyuan, Taiwan, ROC

Jiunn-Jye Sheu and Jui-Ning Yeh contributed equally to this article.

Sponsorships or competing interests that may be relevant to content are disclosed at the end of this article.

*Corresponding author. Address: Division of Cardiology, Department of Internal Medicine, Kaohsiung Chang Gung Memorial Hospital and Chang Gung University College of Medicine, 123, Dapi Road, Niaosung, Kaohsiung 833401, Taiwan, ROC. Tel.: +886 773 171 23; fax: +886 773 224 02. E-mail: han.gung@msa.hinet.net (H.K. Yip).

Copyright © 2024 The Author(s). Published by Wolters Kluwer Health, Inc. This is an open access article distributed under the terms of the Creative Commons Attribution-Non Commercial-No Derivatives License 4.0 (CCBY-NC-ND), where it is permissible to download and share the work provided it is properly cited. The work cannot be changed in any way or used commercially without permission from the journal.

International Journal of Surgery (2024) 110:7546-7562

Received 8 April 2024; Accepted 5 October 2024

Published online 4 November 2024

http://dx.doi.org/10.1097/JS9.0000000000002119

Introduction

Left ventricular (LV) myocardial loss after myocardial infarction (MI) is an irreversible process that results in LV dysfunction, and its severity correlates with infarct size^[1-8]. Notably, a well-established physical phenomenon known as Laplace's law has shown that, under equilibrium conditions, the wall stress (WS) [a parameter of force (F)] tangent to the circumference of a vessel is proportional (α) to its radius to the fourth power (r^4) as in the mathematical expression $F^{WS} \propto r^4$. The equation signifies a substantial elevation of WS associated with only a minor increase in radius. The law also applies to the heart, which is a spherical organ whose weakened LV-free wall after MI causes an increase in LV radius that results in an elevation of LV pressure and further dilatation of the LV chamber. Such a vicious cycle, called LV remodeling, leads to progressive and incessant LV dilatation accompanied by myocardial apoptosis and death that contribute to LV dysfunction with the clinical presentations of heart failure (HF). LV remodeling and HF after IM are considered considerable and independent predictors of unfavorable prognostic outcomes^[2,4,6]. Therefore, preventing LV dilatation is a key factor for preserving LV function and improving prognostic outcomes after MI.

Abundant evidence supports the ability of mesenchymal stem cells (MSCs) to suppress inflammation and enhance immune privilege, tissue regeneration, and angiogenesis^[9–13], which suggests the feasibility of its clinical application as a novel therapeutic approach to various organ diseases [9-16]. Nevertheless, data from tissue engineering studies focusing on the validity of MSCs delivery through biological scaffolds for myocardial repair and tissue regeneration after MI is limited[17,18]. Improved cardiac performance and suppressed LV remodeling through the 'patching' technique in which stem cells were grown or embedded in a special tissue scaffold to form a 'graft' before being implanted in the infarct or ischemic myocardium have been observed^[17-19]. The mechanistic basis of this technique includes (1) enhancement of myocardial regeneration through enrichment of angiogenetic factors or neovascularization and paracrine effects and (2) mechanical advantage from ventriculoplasty that contributes to a reduction in LV dimension, thereby attenuating WS according to Laplace's law.

Consistent with the results of previous reports^[17,18], an early study from our team has demonstrated significant upregulation of angiogenetic factors, increase in small vessel density, preservation of LV performance, and amelioration of LV remodeling via the application of platelet-rich fibrin scaffolds containing adipose-derived MSCs (ADMSCs) on the infarct myocardium in a rat model immediately after the induction of infarction^[19]. However, our study had two limitations. First, we targeted the acute phase of MI rather than a later stage, as in a real clinical situation. Second, data from small animals may not accurately reflect the pathophysiological features of human beings, suggesting the need for a larger animal model to better simulate human conditions.

The efficacy of shock wave (SW) in improving ischemiainduced organ dysfunction, mainly via the suppression of inflammation and oxidative stress, including the promotion of angiogenesis and tissue regeneration, has been verified^[20–23]. Thus, using cell-based biomaterials to regenerate LV myocardial tissues and architecture, an approach known as 'cardiac tissue engineering,' may offer additional benefits to the enhancement of

HIGHLIGHTS

- Myocardial infarction (MI) is the dominant etiology of mortality in patients for any cause of hospitalization.
- Diminished left ventricular (LV) mass after MI is perpetually irreparable to cause LV remodeling and pump failure, which are strongly and independently predictive of unfavorable prognostic outcomes.
- Shock wave-pretreated adipose-derived mesenchymal stem cells seeded in cell-sheet scaffold therapy offered great benefits in inhibiting inflammation, oxidative stress, cellular apoptosis, and LV remodeling as well as enhancing angiogenesis and tissue regeneration, resulting in improving the LV function.

tissue regeneration and inhibition of LV remodeling, thereby improving LV function and prognostic outcomes.

Methods

Ethical statement

All animal experimental protocols and procedures were approved by the Institute of Animal Care and Use Committee (IACUC) at Kaohsiung Chang Gung Memorial Hospital. Animals were housed in an AAALAC-approved animal facility in our hospital (IACUC protocol no. 2019031904). This work has been reported in accordance with the guidelines of Animals in Research: Reporting In Vivo Experiments^[24].

Porcine MI induction and animal grouping

Each male mini-pig (Taitung Animal Propagation Station, Livestock Research Institute, Taiwan), weighing 18–20 kg, was anesthetized by intramuscular injection of ketamine (15 mg/kg) and maintained under anesthesia by inhalation of 1.5% isoflurane. After being shaved on the chest, the mini-pig was placed in the supine position on a warming pad at 37°C and then given endotracheal intubation with positive-pressure ventilation (180 ml/min) with room air using ventilator support (Sn: Q422ZO; SIMS PneuPAC, Ltd.) during the procedure. An electrocardiogram (ECG) monitor and defibrillator were connected to the chest wall of each mini-pig. One ampoule of amiodarone (150 mg) was intravenously administered to each animal before acute myocardial infarction (AMI) induction to prevent malignant arrhythmia.

Under sterile conditions, the heart was exposed using a surgical sternum saw (Stryker 6207 Sternum Saw-MedRepair LLC) to open the sternum through a mid-thoracotomy (through a median sternotomy). The pericardium was then gently incised in a small zone (~3–5 cm) to prevent future adhesion between the chest wall and pericardium, and the midportion of the left anterior descending artery (LAD) was firmly ligated with a 5-0 prolene suture distal to the first diagonal branch. Regional myocardial ischemia was confirmed by typical changes in the waveform on ECG monitoring and observation of rapid discoloration of the myocardium from pink to gray over the anterior surface of the left ventricle, together with the rapid development of akinesia and dilatation of at-risk areas. Following this procedure, AMI was confirmed

using ECG. After the procedure, the sternum and muscle layers were fixed with 1-0 vicryl, followed by 2-0 vicryl sutures for the skin layer.

Mid-LAD ligation was performed in 20 mini-pigs. Two mini-pigs succumbed to either ventricular tachycardia or ventricular fibrillation, even after defibrillation during the LAD-ligated procedure. The remaining 18 mini-pigs were categorized into different groups.

By the 14th day after AMI induction (defined as old MI), the animals (n = 18) in stable condition were equally categorized into group 2 (old MI + intra-myocardium injection of 1.5 ml culture medium), group 3 [old MI + autologous ADMSCs/1.0×10⁷ cells seeded in cell-sheet scaffold (CSS)/embedded into the LV infarcted area], and group 4 (old MI + SW-pretreated ADMSCs/1.0×10⁷ cells, followed by seeding in CSS/embedded into the LV infarcted area). Five healthy mini-pigs served as sham controls (group 1). The sample size of the present study was based on the results of our recent study on MI in mini-pigs treated with human bone marrowderived MSCs^[25] and our previous studies^[26,27] and was calculated by a statistician. The LV ejection fraction (LVEF) of MI mini-pigs without any treatment was $40 \pm 5\%$ 3 months after MI induction. The LVEF in the group of MI mini-pigs after receiving human bone marrow-derived MSCs was improved to $50\% \pm 5\%$. Accordingly, the same size was calculated as 6 in each MI group based on the two-tail effective size = 2.0, α = 0.05, and power = 80%. In consideration of possible death from the MI procedure, 20 mini-pigs were used for this experimental MI study. However, another rationale for using mini-pigs (large animals) to create an old MI model in the present study was to mimic the clinical features of humans with old MI because mini-pigs have similar physiological and anatomical features as humans.

On day 90 after the first thoracotomy, the chest wall was reopened (second thoracic procedure) using the same method the first time for CSS and CSS-ADMSCs embedded into the LV infarcted area. After opening the chest wall, we carefully separated the adhesion between the sternum and pericardium as well as the adhesion in the myocardium by hand with an accessory small scissors commonly used during surgical intervention. After adequate preparation, the CSS and CSS-ADMSCs were embedded into the LV myocardium, followed by careful sutures using the same method as the first time for each animal.

Preparation of autologous fat tissue for the cultivation of ADMSCs

To obtain ADMSCs, adipose tissue was separated from the minipigs on day 14 after AMI induction. The preparation and culture of ADMSCs have been previously described in detail^[9–11,13].

SW treatment for ADMSCs and CSS patched into the infarction zone of the LV myocardium after the open chest wall procedure

The ADMSCs were first seeded in a 25T flask and incubated for 24 h, followed by SW (0.12 mJ/mm² for 140 shots) applied to the flask and incubated for another 24 h. After that, the ADMSCs (1.2×10⁷ cells) were collected and mixed with the temperature-sensitive plasticity gel (TSPG; Industrial Technology Research Institute, Taiwan) that is liquid at \leq 4.0°C and solid at > 4.0°C when exposed for > 6 min. The TSPG was added to a 3.5 cm plate and allowed to stand for 25 min at room temperature. Finally, ADMSCs were incubated for 24 h at 37°C to form an elastic 'CSS.'

In the current study, the interval of day 28 after AMI was defined as the pathological time of the old MI. Accordingly, on day 28 after AMI and immediately after the preparation of ADMSCs cultivated in the CSS, the chest walls of the mini-pigs in groups 2–4 were reopened under anesthesia. The culture medium was then injected into the infarcted and peri-infarcted areas in group 2 mini-pigs, whereas the CSS was firmly patched by several sutured points over the infarcted area of the LV myocardium. This created a framework similar to a splint for fixation after a bone fracture, resulting in the creation of an external compression force that subsequently reduced the WS force. During the procedure, one animal died in groups 2, 3, and 4 each. After the procedure, the mini-pigs recovered from anesthesia and were intensively taken care of for 24 h, and their vital signs were observed.

Evaluation of cardiac function using 2D echocardiography

The methodology for evaluating cardiac function has been described in our previous studies^[20,21,26,27]. Echocardiography was conducted before AMI induction and on days 28, 60, and 180 after the procedure using iE33 (Philips Medical System, Bothell, Washington, USA) with S5 transducers. The LVEF was calculated as follows: LVEF (%) = [(LVEDd³ – LVESd³)/LVEDd³] ×100. A 2D echo performance was assessed by a veterinary cardiologist blinded to the therapeutic strategy.

Specimen preparation and assessment of the infarct area (IA) at the basal, middle, and apical levels of LV

By the 180th day after AMI induction, all the mini-pigs were euthanized after echocardiography. The methodology for IA assessment has been previously reported [20,21,26,27]. Three cross-sections (1 cm-thick) from the basal, middle, and apical levels were used to quantify IA in each animal after staining with 2% triphenyl tetrazolium chloride. Three sections at each level (apical, middle, and basal) of the LV anatomical structure were selected to avoid selection bias in the pathological analysis. Sections were photographed from a fixed height directly above. The obtained images were analyzed using Image Tool 3 (IT3) image analysis software (University of Texas, Health Science Center, San Antonio, UTHSCSA; Image Tool for Windows, Version 3.0, USA) to avoid selection bias. The pathological assessment was conducted by a senior technician blinded to the therapeutic strategy.

Assessment of thickness of the infarcted wall at the papillary muscle level

To elucidate the effect of SW-ADMSCs therapy on myocardial regeneration, three cross-sections of the LV at the papillary muscle level were used with the three thickest regions chosen, and the thickness was calculated for each mini-pig. Data were further summarized and divided into six groups for statistical analysis. The papillary muscle level was used as an estimation of wall thickness because most cases of MI-induced myocardial necrosis or ischemia are predominantly distributed in these levels of the LV-free wall. The pathological parameters were determined by a senior technician blinded to the therapeutic strategy.

Assessment of small vessels in infarct and peri-infarct areas

This methodology has been previously described^[20,26,27]. Estimation of the small vessel density in the infarct and peri-infarct areas at the papillary muscle level was used to determine

the capacity for angiogenesis or neovascularization after SW + CSS-ADMSCs therapy. Three sections of the basal, middle, and apical levels of the LV myocardium, which were selected for immunohistochemical (IHC) staining for small vessel density, were treated with alpha-smooth muscle actin (α -SMA; 1:400) as the primary antibody at room temperature for 1 h, followed by rinsing with phosphate-buffered saline (PBS) thrice. The antimouse-horseradish peroxide (HRP)-conjugated secondary antibody was then added for 10 min, followed by rinsing with PBS thrice. Hematoxylin and eosin (H&E) staining was performed by a senior technician blinded to the therapeutic strategy.

Pathohistological examination of fibrosis in IAs

This methodology has been previously described [20,26,27]. Masson's trichrome staining was used to evaluate LV myocardial fibrosis. Three serial sections of the LV myocardium at the basal, middle, and apical levels of the left ventricle were prepared at 4 μ m thickness using a Cryostat (Leica CM3050S). We estimated the IAs to select these anatomical levels. The integrated area (μ m²) of fibrosis in the slides was calculated using the IT3 image analysis software. Three sections from each animal were quantified. The mean pixel number per high-power field (HPF) for each mini-pig was then calculated by summing all the pixel numbers and dividing them by nine. The mean integrated area (μ m²) of fibrosis in the LV myocardium per HPF was determined using a conversion factor of 19.24 (1 μ m² represented 19.24 pixels). Masson's trichrome staining was performed by a senior technician blinded to the therapeutic strategy.

IHC staining

This methodology was previously reported [$^{10-13}$]. Rehydrated paraffin sections were treated with 3% H_2O_2 for 30 min and incubated with an ImmunoBlock reagent for 30 min at room temperature. Sections were then incubated with primary antibodies specifically against α -SMA (1:400, Sigma Aldrich) and r-H2AX (1:1000, Abcam). Sections incubated with irrelevant antibodies served as controls.

Western blot

The procedure and protocol have been previously described^[10-13]. Equal amounts (50 µg) of protein extracts were loaded and separated by sodium dodecyl sulfate-polyacrylamide gel electrophoresis using 8-12% acrylamide gradients. After electrophoresis, the separated proteins were transferred onto a polyvinylidene difluoride membrane (Amersham Biosciences). Nonspecific sites were blocked by incubating the membrane in a blocking buffer (5% nonfat dry milk in Tris-buffered saline containing 0.05% Tween 20) at room temperature for 30 minutes. The membranes were incubated with the indicated primary antibodies [vascular endothelial growth factor (VEGF; 1:1000, Abcam), stromal cell-derived factor-1α (SDF-1α; 1:1000, Cell Signaling), C-X-C chemokine receptor type 4 (CXCR4; 1:1000, Abcam), angioetin-1 (1:1000, Abcam), bone morphogenetic protein-2 (BMP-2; 1:1000, Abcam), phosphorylated Smad1/5 (1:1000, Cell Signaling), von Willebrand factor (vWF; 1:1000, Abcam), endothelial nitric oxide synthase (eNOS; 1:1000, Abcam), angiopoietin-1 (1:1000, Abcam), cytosolic cytochrome (1:5000, BD), mitochondrial cytochrome C (1:5000, BD), γ-H2AX (1:1000, Cell Signaling), phosphorylated Smad3 (1:1000, Cell Signaling), transforming growth factor β (TGF)-β (1:1000, Abcam), complex I (1:5000, Abcam), complex II (1:5000, Abcam), complex III (1:5000, Abcam), complex IV (1:5000, Abcam), complex V (1:5000, Abcam), matrix metalloproteinase-9 (MMP-9; 1:1000, Abcam), interleukin-6 (IL-6; 1:1000, Abcam), cyclooxygenase-2 ([COX-2; 1:1000, Abcam), interferon gamma (IFN-γ; 1:1000, Abcam), NADPH oxidase (NOX-1; 1:1000, Sigma), NOX-2 (1:1000, Sigma), mitochondria respiratory chain (MRC I; 1:5000, Abcam), MRC II (1:5000, Abcam), MRC III (1:5000, Abcam), and MRC IV (1:5000, Abcam)] for 1 h at room temperature. HRP-conjugated antirabbit immunoglobulin G (1:2000, Cell Signaling Technology) was used as the secondary antibody for the 1 h incubation at room temperature. The rinsing procedure was repeated eight times within 1 h, and the immunoreactive bands were visualized chemiluminescence enhanced (ECL; Amersham Biosciences) after exposure to Biomax L film (Kodak). ECL signals were digitized using the Labwork software (UVP) for quantification.

Statistical analysis

All parameters were expressed as mean \pm standard deviation. The differences between the two groups were compared using Student's *t*-test. Additionally, continuous variables among different groups were compared using analysis of variance (ANOVA), followed by the Bonferroni test for post hoc betweengroup comparison. However, repeated measures of ANOVA were adopted to analyze cell variability at different time points. Statistical analysis system (SAS) software for Windows version 8.2 (SAS Institute, Cary, North Carolina, USA) was used as an analytic tool. Statistical significance was set at P < 0.05.

Results

In-vitro study to verify the effect of SW and ADMSCs on attenuating the inflammatory reaction, oxidative stress, and apoptosis

To verify the therapeutic effect of SW and ADMSCs on ameliorating inflammation and oxidative stress, Raw 264.7 Cells (mouse mononuclear macrophages) were categorized into four groups: A1 (Raw 264.7 Cells), A2 [Raw 264.7 Cells + lipopolysaccharide (LPS: 50 ng/ml)], A3 [Raw 264.7 Cells + LPS + pig-derived ADMSCs $(5.0 \times 10^5 \text{ cells})$], and A4 (Raw 264.7 Cells + LPS + SW (0.12 mJ/ mm² for a total of 140 shots)] + pretreated pig-derived ADMSCs (5.0×10^{3}) cells). The results showed that the protein levels of matrix metalloproteinase-9 (MMP-9), IL-6, COX-2, and IFN-y, four indices of inflammation, protein levels of NOX-1 and NOX-2, and two biomarkers of oxidative stress were most significantly lower in A1, the highest in A2, and remarkably higher in A3 than in A4. Flow cytometry revealed that early and late apoptosis had similar MMP-9 expression among the groups. Furthermore, flow cytometry revealed that the surface expression of M1 in macrophages, an index of inflammation, was most significantly lower in A1, greatly upregulated in A2 compared with A3 and A4, and notably higher in A3 than in A4. In contrast, the surface expression of M2 in macrophages, an index of anti-inflammation, significantly and gradually increased from A1 to A4. Thus, the ratio of M2 to M1 was reduced most in A2, the highest in A4, and significantly higher in A1 than in A3, implying that combination therapy with SW and

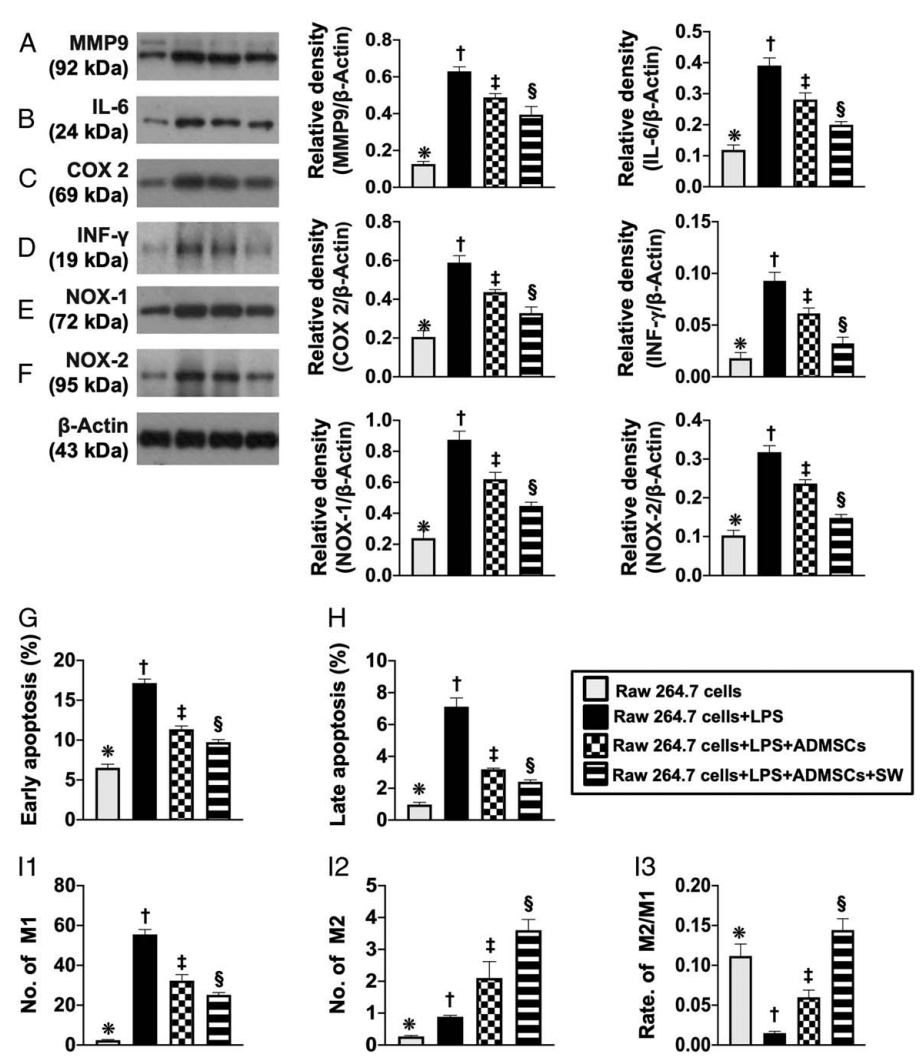


Figure 1. Effect of SW and ADMSCs on alleviating inflammation, oxidative stress and apoptosis. (A) Western blot result of MMP-9, * versus other groups with different symbols (\uparrow , \uparrow , \S), P < 0.0001. (B) Western blot result of interleukin (IL)-6, * versus other groups with different symbols (\uparrow , \uparrow , \S), P < 0.0001. (C) Western blot result of COX-2, * versus other groups with different symbols (\uparrow , \uparrow , \S), P < 0.0001. (E) Western blot result of NOX-1, * versus other groups with different symbols (\uparrow , \uparrow , \S), P < 0.0001. (F) Western blot result of NOX-2, * versus other groups with different symbols (\uparrow , \uparrow , \S), P < 0.0001. (G) Flow cytometric assessment of early (AN-V⁺/PI⁻) apoptosis, * versus other groups with different symbols (\uparrow , \uparrow , \S), P < 0.0001. (H) Flow cytometric assessment of late (AN-V⁺/PI⁺) apoptosis, * versus other groups with different symbols (\uparrow , \uparrow , \S), P < 0.0001. (H-1) Number of M1 surface expression in Raw 264.7 Cells, * versus other groups with different symbols (\uparrow , \uparrow , \S), P < 0.0001. (H-2) Number of M2 surface expression in Raw 264.7 Cells, * versus other groups with different symbols (\uparrow , \uparrow , \downarrow), \uparrow 0.0001. (H-2) Number of M2 surface expression in Raw 264.7 Cells, * versus other groups with different symbols (\uparrow , \uparrow , \downarrow), \downarrow 0.0001. (H-2) Number of M2 surface expression in Raw 264.7 Cells, * versus other groups with different symbols (\uparrow , \uparrow , \downarrow), \downarrow 0.0001. (H-3) Ratio of M2/M1, * versus other groups with different symbols (\uparrow , \uparrow , \downarrow 0.0001. (H-3) Ratio of M2/M1, * versus other groups with different symbols (\uparrow 0.05 level). ADMSCs, adipose-derived mesenchymal stem cells; LPS, lipopolysaccharide; SW, shock wave.

ADMSCs was superior to a single therapy for reducing inflammation and oxidative stress (Fig. 1).

SW treatment augmented cell proliferation, angiogenesis biomarkers, and the manifestation of mitochondrial cytochrome C in ADMSCs

To elucidate whether SW treatment could augment cell proliferation, angiogenesis biomarker ability, and the expression of mitochondrial cytochrome C, ADMSCs were categorized as B1 (ADMSCs only) and B2 [ADMSCs + SW (0.12 mJ/mm² for 140 shots)]. The triphenyl tetrazolium chloride (TTC) assay showed that cell viability was markedly higher in B2 than in B1 at 24, 48, and 72 h. Additionally, microscopic examination revealed that the level

of mitochondrial cytochrome C in ADMCSs was higher in B2 than in B1. The protein levels of VEGF and SDF-1 in ADMSCs, two angiogenesis biomarkers, and the cellular expression of Ki67, an indicator of proliferation, were notably higher in B2 than in B1 (Fig. 2).

SW treatment upregulated the expression of relative mitochondrial DNA (mtDNA), adenosine triphosphate (ATP) concentration, mitochondrial bioenergetics, and the expression of respiratory chain complexes in ADMSCs

According to the findings shown in Figure 2, SW treatment upregulated ADMSCs proliferation, and we used the cell grouping of B1 and B2 to verify whether the mitochondrial

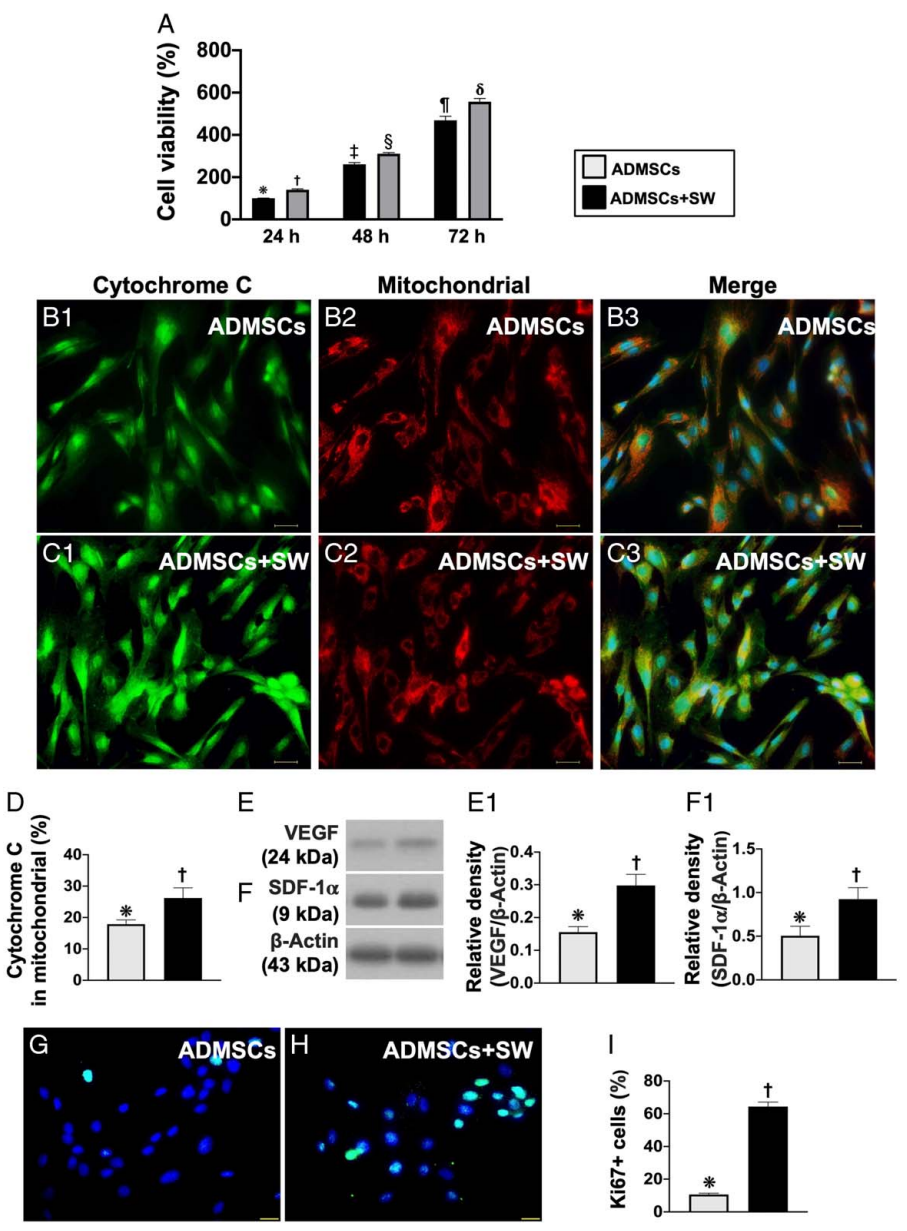


Figure 2. SW treatment augmented cell proliferation ability, number of mitochondrial cytochrome C, and angiogenesis biomarkers in ADMSCs. (A) Cell viability at 24 h, * versus †, P < 0.0001. (B) Cell viability at 48 h, ‡ versus §, P < 0.0001. (C) Cell viability at 72 h, ¶ versus δ , P < 0.00001. Note that the repeated measures ANOVA was adopted to analyze cell variability at different time points. (D1–D3 and E1–E3) Showing the immunofluorescent microscopic finding (400x) for identifying the expression of mitochondrial cytochrome C (red-green color in the merged picture). (D1 and E1) Indicated the cytochrome C stain (green color); (D2 and E2) Indicated mitochondrial stain (red color); (D3 and E3) Indicated the merged picture of A and B (red-green color). (F) The percentage (%) of positively stained cytochrome C in mitochondria, * versus †, P < 0.0001. (G) Western blot analysis of VEGF, * versus †, P < 0.0001. (H) Western blot analysis of SDF-1 α , * versus †, P < 0.0001. n = 6 in each group. (I and J) Demonstrating the IF microscopic finding (400x) for identifying the cellular expression of Ki68 (green color). (K) Analytical result of the number of Ki67+ cells, * versus †, P < 0.0001. n = 4 in each group.

content, oxygen consumption rate, and ATP would also be upregulated by SW treatment. As expected, relative mtDNA, an index of mitochondrial integrity, was remarkably upregulated in B2 compared to that in B1. Additionally, ATP concentration was significantly higher in B2 than in B1 (Fig. 3).

Furthermore, to estimate the impact of SW on mitochondrial respiration, groups B1 and B2 were subjected to a Seahorse XF24 extracellular flux analyzer to assess the efficiency of mitochondrial respiration, reflected by the OCR, which is an indicator of

effective mitochondrial utilization. Significant progressive increases were observed in mitochondrial respiration, including basal and maximal respiration, ATP generation, and spare respiration capacity, indicating that mitochondrial bioenergetics were better in B2 than in B1.

The protein expression of mitochondrial respiration chains of complexes I, II, III, and IV was substantially increased in B2 compared to that in B1. These findings implied that the SW treatment enhanced ADMSCs proliferation, resulting in the

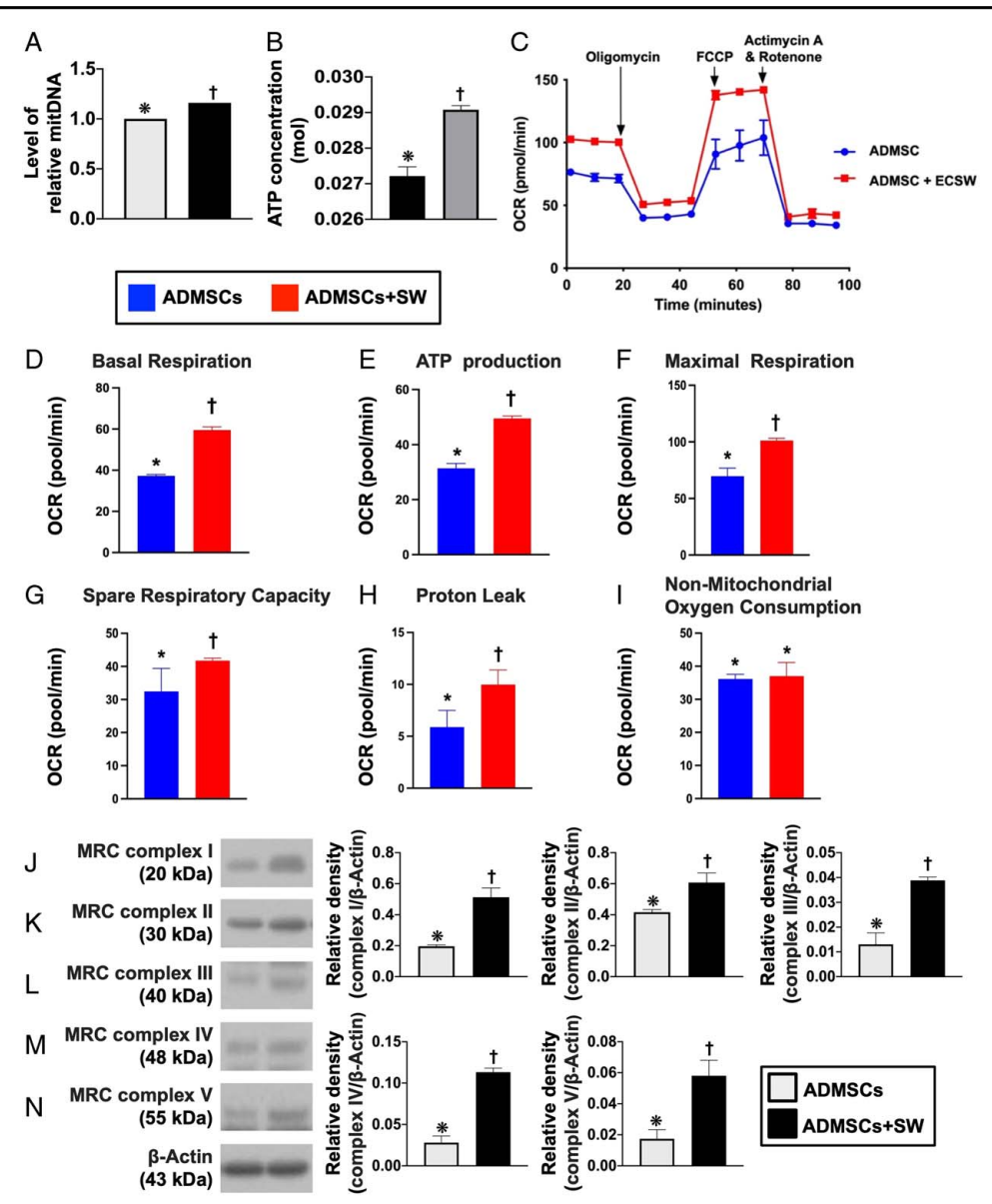


Figure 3. SW treatment augmented the expressions of relative mitochondrial DNA (mtDNA), ATP concentration, mitochondrial bioenergetics, and expressions of respiratory chain complexes in the ADMSCs. (A) Level of relative mtDNA, *versus †, P < 0.0001. (B) The ATP concentration, *versus †, P < 0.0001. (C to I) Changes in mitochondrial respiration of ADMSCs with and without SW treatment. (C) Indicated mitochondria respiration reflected by the level of oxygen consumption rate (OCR) in B1 and B2, following the injection of oligomycin, FCCP, and antimycin A/rotenone (Back. corr. = Background correction). (D) The rates of basal respiration, (E) ATP production, (F) maximal respiration, (G) spare respiratory capacity (n = 4 per group), and (H) protein leakage, respectively; * versus †, all P < 0.0001. (I) Non-mitochondrial oxygen consumption, P > 0.5. (J) Western blot analysis of mitochondria respiratory chain (MRC) complex I, * versus †, all P < 0.0001. (L) Protein expression of MRC complex III, * versus †, all P < 0.0001. (M) Western blot analysis of MRC complex V, * versus †, all P < 0.0001. (M) Western blot analysis of MRC complex V, * versus †, all P < 0.0001. (M) Western blot analysis of MRC complex V, * versus †, all P < 0.0001. (M) Western blot analysis of MRC complex V, * versus †, all P < 0.0001. (M) Western blot analysis of MRC complex V, * versus †, all P < 0.0001. (M) Western blot analysis of MRC complex V, * versus †, all P < 0.0001. (M) Western blot analysis of MRC complex V, * versus †, all P < 0.0001.

upregulation of relative mitochondrial DNA, OCR, ATP, and electron transport chain efficacy in ADMSCs.

Comparison of the growth morphological feature of ADMSCs between Matrigel, hyaluronic acid, and TSPG

To verify whether the growth ability of ADMSCs in TSPG was not inferior to that of Matrigel and hyaluronic acid, the same number of ADMSCs derived from the 24-h cell culture from those isolated from autologous adipose tissues was mixed with the materials previously listed and incubated under the same

conditions of temperature and culture medium. On the 7th day of cell culture, microscopic examination revealed similar numbers and morphological features of ADMSCs, indicating that TSPG was suitable for ADMSCs growth and proliferation. (Fig. 4)

Accumulation of mortality rate at the end of the study period and measurement of time courses of LVEF using transthoracic echocardiography

In total, 25 animals were used in this study. The mortality rate during AMI induction (at the first time point of the procedure)

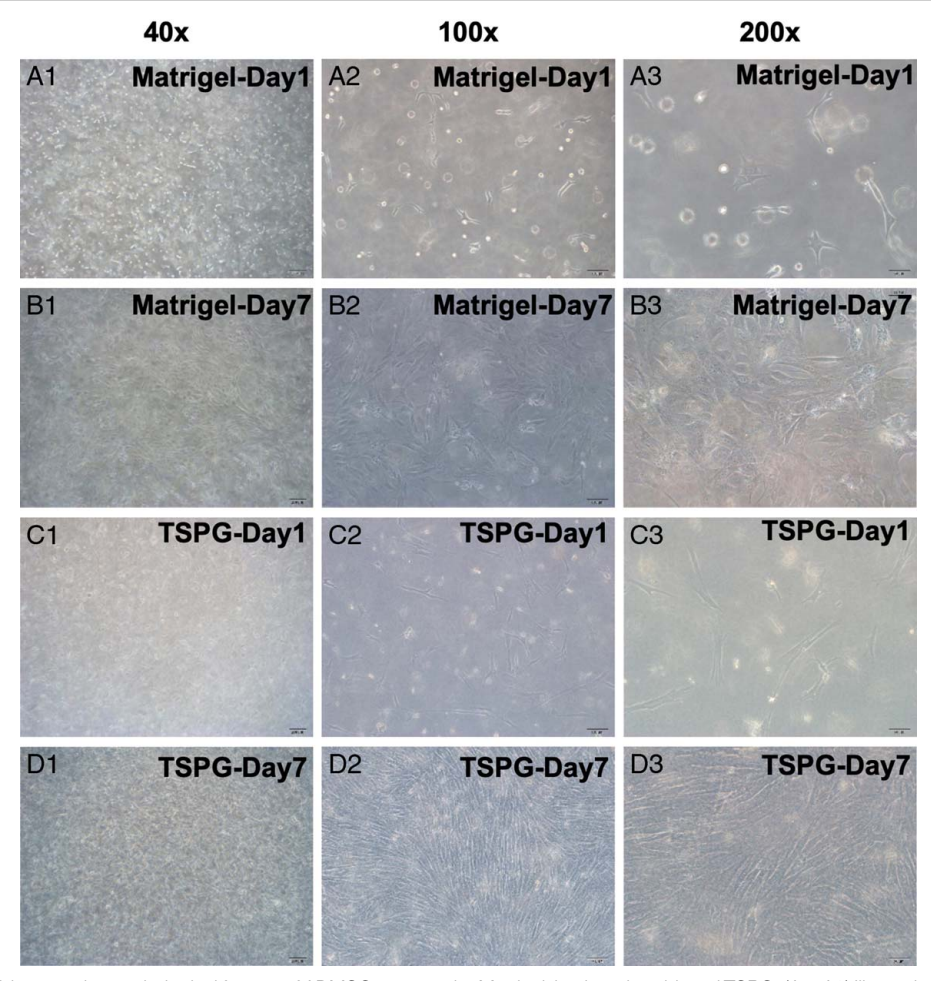


Figure 4. Comparison of the growth morphological feature of ADMSCs among the Matrigel, hyaluronic acid, and TSPG. (A1–A3) Illustrating the morphologic feature of ADMSCs after 24 h of culture in Matrigel culture plate, that is, at 40× (A1), 100× (A2), and 200× (A3), respectively. (B1–B3) Illustrating the morphologic feature (i.e. typical spindle shape) of ADMSCs after 7 days culture in Matrigel culture plate, that is, at 40× (B1), 100× (B2), and 200× (B3), respectively. (C1–C3) Illustrating the morphologic feature of ADMSCs after 24 h of culture in TSPG culture plate, that is, at 40× (C1), 100× (C2), and 200× (C3), respectively. (D1–D3) Illustrating the morphologic feature (i.e. typical spindle shape) of ADMSCs after 7 days of culture in TSPG culture plate, that is, at 40× (D1), 100× (D2), and 200× (D3), respectively. TSPG, temperature-sensitive plasticity gel.

was 8% (2/25). The mortality rate during the second procedure before the final animal grouping was 13.04% (3/23). No further deaths occurred until the end of the study period. Thus, the cumulative mortality rate in this study was 20% (5/25) (Table 1).

To elucidate whether SW-pretreated ADMSCs in CSS could provide additional advantages in preserving LV function, transthoracic echocardiography (2D M-mode method) was adopted in the current study, and LVEF, fractional shortening (FS), LVESD, and LVEDD at baseline, on day 28 (prior to ADMSCs treatment), and 60 and 180 days after AMI induction were derived.

The baseline values of LVEF, FS, LVESD, and LVEDD did not differ between groups 1 (SC), 2 (old MI), 3 (old MI + autologous ADMSCs seeded in CSS), and 4 (old MI + SW-pretreated ADMSCs seeded in CSS). However, by the 28th day after AMI induction, LVEF and FS remarkably increased, whereas LVESD and LVEDD remarkably decreased in group 1 compared with those in the other three groups. These parameters did not differ between groups 2 and 4 at this time point.

On day 60 after AMI induction, LVEF increased the most in group 1, decreased the most in group 2, and increased notably in group 4 compared with group 3. FS was notably higher in group 1 than in groups 2–4 and was notably increased in groups 3 and 4 compared with group 2. However, FS was similar between groups 3 and 4. In contrast, LVESD and LVEDD were remarkably lower in group 1 than in groups 2–4 and remarkably lower in groups 3 and 4 than in group 2. They were similar in groups 3 and 4.

On day 180 after AMI induction, LVEF and FS increased the most in group 1, decreased the most in group 2, and significantly increased in group 4 compared with group 3. In contrast, LVESD and LVEDD, two indices of LV remodeling, were significantly lower in groups 1, 3, and 4 than in group 2; however, no difference was observed between groups 3 and 4.

These findings imply that SW-pretreated autologous ADMSCs seeded in CSS were superior to autologous ADMSCs seeded in CSS in preserving LV function and reducing LV chamber size parameters of LVESD and LVEDD (defined as reducing the LV remodeling).

Table 1
Serial changes of LVEF were assessed by transthoracic echocardiography.

Variable	Group 1 (<i>n</i> = 5)	Group 2 (<i>n</i> =5)	Group 3 (<i>n</i> = 5)	Group 4 (<i>n</i> = 5)	P*
Baseline					
LVEDd (mm)	28.14 ± 1.64	30.64 ± 2.51	29.09 ± 3.34	29.68 ± 3.78	> 0.2
LVESd (mm)	17.95 ± 1.22	18.3333 ± 4.64	18.54 ± 2.24	19.27 ± 1.85	> 0.3
LVEF (%)	67.73 ± 1.26	67.2267 ± 2.55	67.73 ± 0.93	67.8 ± 1.37	> 0.7
FS (%)	35.83 ± 2.29	36.1 ± 1.9	36.29 ± 0.55	36.69 ± 1.09	> 0.5
At day 28					
LVEDd (mm)	29.98 ± 1.97^{a}	34.83 ± 9.69^{b}	34.81 ± 5.19 ^b	34.73 ± 4.47^{b}	< 0.001
LVESd (mm)	19.44 ± 1.57^{a}	28.47 ± 3.68^{b}	27.49 ± 4.11 ^b	26.34 ± 3.58^{b}	< 0.0001
LVEF (%)	66.12 ± 1.92^{a}	46.49 ± 3.54^{b}	46.11 ± 1.94 ^b	47.43 ± 3.43^{b}	< 0.0001
FS (%)	35.2 ± 1.32^{a}	22.73 ± 2.13^{b}	21.99 ± 1.25^{b}	23.37 ± 1.88^{b}	< 0.0001
At day 60					
LVEDd (mm)	32.04 ± 2.22^{a}	43.12 ± 7.63^{b}	$36.09 \pm 3.46^{\circ}$	$36.82 \pm 5.41^{\circ}$	< 0.0001
LVESd (mm)	20.83 ± 1.78^{a}	32.10 ± 4.89^{b}	$26.6 \pm 1.74^{\circ}$	$26.09 \pm 3.90^{\circ}$	< 0.0001
LVEF (%)	65.68 ± 2.32^{a}	46.25 ± 4.77^{b}	51.94 ± 4.84^{c}	56.83 ± 2.37^{d}	< 0.0001
FS (%)	35.06 ± 1.61^{a}	22.99 ± 3.07^{b}	$26.03 \pm 3.22^{\circ}$	29.13 ± 1.54^{c}	< 0.0001
At day 180					
LVEDd (mm)	32.16 ± 2.47^{a}	42.91 ± 8.08^{b}	36 ± 4.51^{c}	$37.93 \pm 4.64^{\circ}$	< 0.0001
LVESd (mm)	20.78 ± 1.94^{a}	33.99 ± 6.45^{b}	27.78 ± 3.65^{c}	$26.11 \pm 2.85^{\circ}$	< 0.0001
LVEF (%)	66.57 ± 2.60^a	44.35 ± 3.37^{b}	56.07 ± 3.90^{c}	61.38 ± 3.12^{d}	< 0.0001
FS (%)	35.63 ± 1.81^{a}	21.25 ± 1.59^{b}	$28.85 \pm 2.83^{\circ}$	33.51 ± 1.56^{d}	< 0.0001

Data are expressed as mean \pm SD or % (n).

*Indicates by one-way ANOVA. Different letters (a, b, c, d) were used for grouping, indicating significant differences (< 0.05) among different groups by the Bonferroni multiple-comparison post hoc test. ADMSCs, adipose-derived mesenchymal stem cells; FS, fractional shortening; group 1, sham-operated control; group 2, old myocardial infarction (MI); group 3, old MI + cell-sheet scaffold of autologous ADMSCs (1.0×10⁷ cells); group 4, old MI + ECSW pretreated cell-sheet scaffold of autologous ADMSCs (1.0×10⁷ cells); LVEF, left ventricular ejection fraction; LVEDd, left ventricular-end-diastolic dimension; LVESd, left ventricular-end-systolic dimension.

TTC assay for infarcted size, determination of the thickness of the wall and internal LV chamber size in the infarcted zone, and histology of cross-sectioned IAs in infarcted and peri-infarcted zones by the 180th day after AMI induction

To verify the effect of ADMSCs + CSS on the reduction of the infarcted area, infarct sizes at three levels – basal, middle, and apical – were assessed. The IAs of all layers were reduced the most in group 1, increased the most in group 2, and significantly reduced in group 4 compared with group 3. Consistently, the cross-section of the chamber size at the middle LV level revealed a similar infarcted area within the groups. In addition, the wall thickness of the middle cross-section exhibited an opposite pattern of the infarcted areas within the four groups (Fig. 5).

H&E staining was used to determine the cross-sections of infarcted and peri-infarct zones in the present study. Through visual observation of the anatomical structure during harvesting of the LV myocardium, we collected specimens from two distinct areas of the infarcted and peri-infarcted zones. Microscopic examination illustrated that IAs in these two distinctive zones were the lowest in group 1, highest in group 2, and substantially lower in group 4 than in group 3, indicating that SW-pretreated autologous ADMSCs implanted in CSS were superior to autologous ADMSCs implanted in CSS for reducing the infarct size.

Vessel density in infarcted and peri-infarcted areas on day 180 after AMI induction

 α -SMA staining was used to elucidate whether the two innovative treatments would augment the neovascularization of small vessels (\leq 25.0 μ M). The number of small vessels in both infarcted and

peri-infarcted areas increased the most in group 1, reduced the most in group 2, and remarkably increased in group 4 compared with group 3, implying that SW booster in ADMSCs effectively enhanced angiogenesis or vasculogenesis in the ischemic area (Fig. 6).

Fibrosis area and DNA-damage biomarker in infarcted areas on day 180 after AMI induction

Histopathological examination demonstrated that the fibrosis area (identified using Masson's trichrome stain) and γ -H2AX (index of a DNA-damaged biomarker identified using the immunofluorescence stain) were reduced the most in group 1, increased the most in group 2, and significantly lower in group 4 than in group 3. SW-pretreated autologous ADMSCs implanted in CSS were superior to autologous ADMSCs implanted in CSS in reducing myocardial injury (Fig. 7).

Protein levels of angiogenetic factors and integrity of endothelial cell biomarkers in peri-infarcted areas on day 180 after AMI induction

To identify these biomarkers, western blot analysis was conducted *in vivo*. The protein levels of SDF-1α, CXCR4, VEGF, and angiopoietin-1, four indices of angiogenetic markers, were substantially and gradually upregulated from groups 1 to 4, implying an intrinsic response to ischemia stimulation further increased by SW-ADMSCs treatment (Fig. 8).

The protein levels of vWF and eNOS, two indices of endothelial cell surface biomarker integrity, increased the most in group 1, reduced the most in group 2, and notably increased in group 4 compared with group 3.

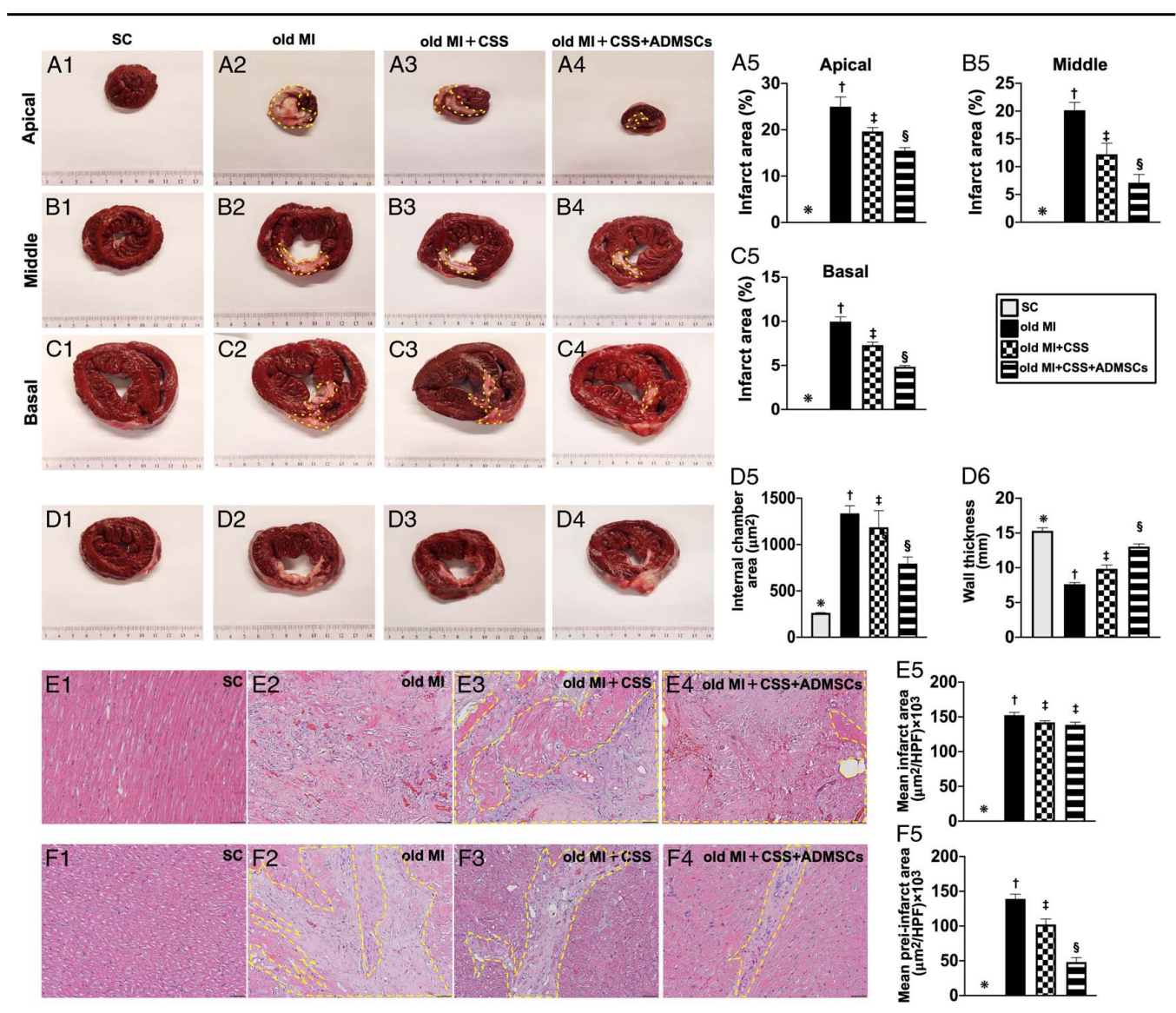


Figure 5. MTT assay for infarcted size, identifications of thickness of the wall, internal LV chamber size in infarcted zone, and histological finding of cross-section infarct areas in infarcted and peri-infarcted zones by 180th day after AMI induction. (A1–A4) Illustrating the MTT assay to identify the infarct area at the apical (yellow dotted line). (A5) Analyzed result of the infarcted area at apical level, * versus other groups with different symbols (†, ‡, §), P < 0.0001. (B1–B4) Illustrating the MTT assessment for clarification of the infarcted area at the middle level (yellow dotted line). (B5) Analyzed result of the infarcted area at the middle level, * versus other groups with different symbols (†, ‡, §), P < 0.0001. (C1–C4) Illustrating the MTT examination for clarifying infarcted area at basal level (yellow dotted line). (C5) Analyzed result of the infarcted area at the basal level, * versus other groups with different symbols (†, ‡, §), P < 0.0001. (D1–D4) Showing the morphological feature of internal chamber size at the middle level of the left ventricle. (D5) Analysis of internal chamber area, * versus other groups with different symbols (†, ‡, §), P < 0.0001. (D6) Analysis of the wall thickness at the middle level of the infarcted zone, * versus other groups with different symbols (†, ‡, §), P < 0.0001. (E1–E4) Microscopic finding (200x) of H&E stain for clarification of peri-infarct area (yellow dotted line). (E5) Analysis of infarct area, * versus other groups with different symbols (†, ‡, §), P < 0.0001. (F1–F4) Microscopic finding (200x) of H&E stain for clarification of peri-infarct area (yellow dotted line). (F5) Analysis of peri-infarct area, * versus other groups. Symbols (†, ‡, §), P < 0.0001. (F1–F4) Microscopic finding (200x) of H&E stain for clarification of peri-infarct area (yellow dotted line). (F5) Analysis of peri-infarct area, * versus other groups. Symbols (†, ‡, §), P < 0.0001. (F1–F4) Microscopic finding (200x) of H&E stain for clarification of peri-infarct

Protein levels related to apoptosis, fibrosis, and mitochondrial or DNA-damaged markers and complexes I–IV in peri-infarcted areas on day 180 after AMI induction

The protein levels of Smad3 and TGF-β, two indices of apoptosis, reduced the most in group 1, increased the most in group 2, and significantly increased in group 3 compared with group 4. In contrast, BMP-2 and Smad1/5, two indices of anti-apoptotic markers, exhibited an antithetical manner of Smad3 within the four groups (Fig. 9).

The protein level of cytosolic cytochrome C, an index of mitochondrial damage, and γ -H2AX, an index of DNA damage, exhibited a similar manner of apoptosis within the four groups. In contrast, those of mitochondrial cytochrome C, an index of mitochondrial integrity, and complexes I–IV, four indicators of functional integrity of electron transport, displayed an opposing manner of cytosolic cytochrome C within the four groups.

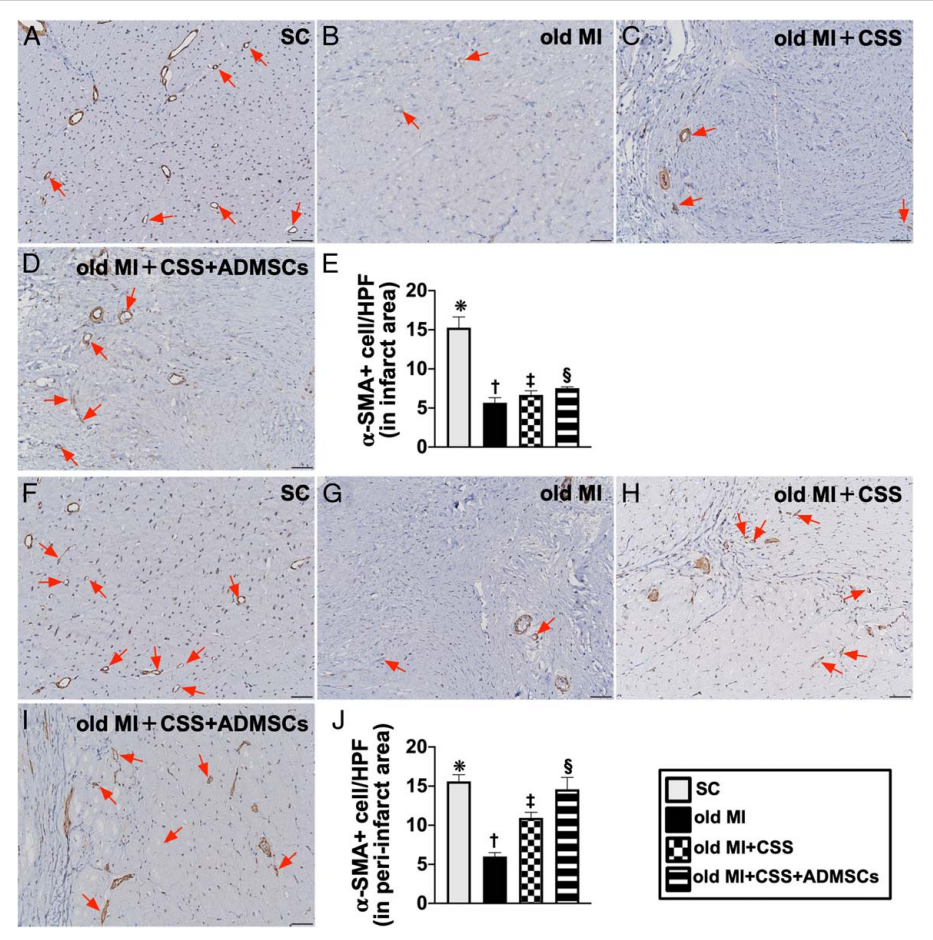


Figure 6. Vessel density in infarcted and peri-infarcted areas and apoptotic nuclei in the infarcted area by 180th day after AMI induction. (A–D) Microscopic finding (200x) of α -SMA stain for identification of small vessels in infarct area (red arrow). (E) Analysis of the number of small vessels (defined as \leq 25.0 μM) in infarct area, * versus other groups with different symbols (†, ‡, §), P < 0.0001. (F–I) Microscopic finding (200x) of α -SMA stain for clarification of small vessels in peri-infarct area (red arrow). (E) Analysis of a number of small vessels (defined as \leq 25.0 μM) in peri-infarct area, * versus other groups with different symbols (†, ‡, §), P < 0.0001. The scale bars in lower right corner represent 50 μm. n = 5 for each group. Symbols (*, †, ‡, §) express significance (at 0.05 level). CSS, cell-sheet scaffold; MI, myocardial infarct.

Quantitative polymerase chain reaction (qPCR) analyses of inflammation, apoptosis, and oxidative stress in peri-infarcted areas on day 180 after AMI induction

Gene expressions were analyzed using qPCR according to the manufacturer's instructions. The qPCR showed that the relative gene expressions of IL-1β, IL-6, and tumor necrosis factor-α, three indices of inflammation, relative gene expressions of NOX-1 and NO-4 and (flavin-containing dimethylaniline mono-oxygenase 2 [FMO2]), three indicators of oxidative stress, and relative gene expression of Bim, an indicator of apoptosis, were highest in group 2, lowest in group 1 and significantly lower in group 4 than in group 3. However, the relative gene expressions of Bcl-2 and Bcl-xL, two biomarkers of anti-apoptosis, displayed an opposite pattern of inflammation among the groups (Fig. 10).

Discussion

This study investigated SW-pretreated ADMSCs seeded in CSS using a large animal model of old MI, followed by patching on the surface of the LV IA, resulting in several preclinical striking implications. First, by permanent ligation of the LAD, we

successfully created a large animal model of old MI; the LV chamber size (LVEDd and LVESd) notably increased progressively in old MI animals, which strongly supports a pathological scenario of LV remodeling. Second, a novel finding of the current study was that SW-pretreated ADMSCs + CSS were superior to ADMSCs + CSS in preserving LV performance and suppressing LV remodeling. Third, we confirmed that improving LV performance and suppressing LV remodeling in old MI pigs could be mainly achieved with the combined effect of the ADMSCs treatment (enhancing angiogenesis and altering cellular-molecular perturbations) and CSS patching (providing a force for limiting the dilatation of the LV chamber), resulting in reduced LV WS force and vanishing LV remodeling (Laplace's law phenomenon).

The role of tissue regeneration of SW has been extensively investigated in previous studies^[20–23,26–28]. Several novel findings were observed in our in-vitro study. First, SW treatment significantly suppressed inflammation, oxidative stress, and apoptosis. Second, SW treatment augmented ADMSCs proliferation and generated angiogenesis biomarkers. Third, SW treatment upregulated the mitochondrial number and ATP concentration in ADMSCs and the efficacy of mitochondrial oxidative phosphorylation and mtDNA copy number. These findings encouraged us

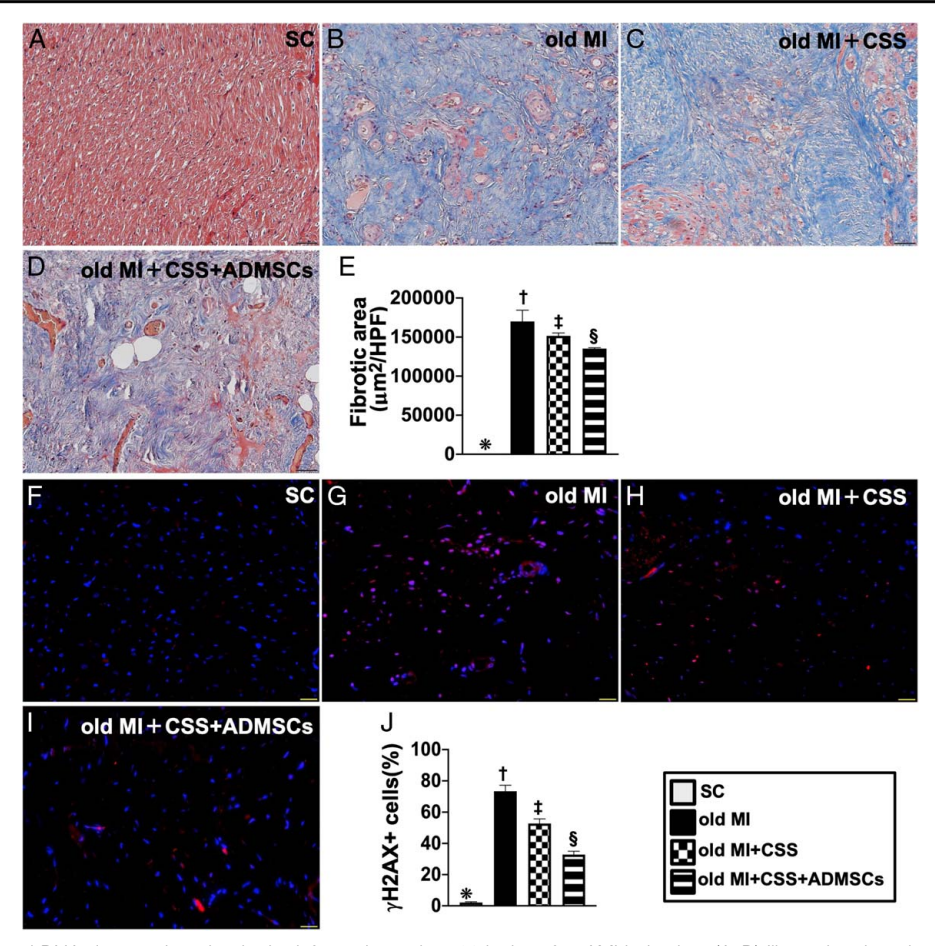


Figure 7. Fibrosis area and DNA-damaged marker in the infarcted area by 180th day after AMI induction. (A–D) Illustrating the microscopic finding (200x) of Masson's trichrome stain for clarification of fibrosis area (blue area). (E) Analytical result of fibrotic area, * versus other groups with different symbols (†, ‡, §), P < 0.0001. (F–I) Demonstrating the IF microscopic finding (200x) for identifying the positively stained γ-HA2X cells (pink color). (J) Analysis of γ-HA2X+ cells, * versus other groups with different symbols (†, ‡, §), P < 0.0001. The scale bars in lower right corner represent 50 μm. n = 5 for each group. Symbols (*, †, ‡, §) express significance (at 0.05 level). CSS, cell-sheet scaffold; MI, myocardial infarct.

to use SW-pretreated ADMSCs prior to seeding in the TSPG to form a CSS to enhance tissue regenerative therapy in the present in-vivo study.

The relationship between old MI and endless LV remodeling has been extensively investigated^[1-8]. Consequently, it causes decompensated HF and extremely poor long-term prognostic outcomes, even with advanced pharmacomodulation[1-8,29,30]. Notably, compared to the SC group, the LVEDd and LVESd parameters measured on serial echocardiography on days 28, 60, and 180 significantly and progressively increased in the old MI group. Additionally, anatomical findings on day 180 showed that the LV chamber size was notably increased, whereas LVEF was remarkably reduced in the old MI group compared with the control group. Our results, aside from supporting previous reports^[1-8], create a platform for an old MI animal model to investigate different management strategies for inhibiting LV remodeling. The most cardinal finding in the current study was that, compared with that in the old MI group, the LV chamber size was remarkably reduced in old MI animals treated with ADMSCs + CSS and significantly reduced in old MI animals treated with SW-pretreated ADMSCs + CSS. In contrast, the LVEF showed an opposing pattern of LV chamber size within the three groups. Our findings highlight that the combination of ADMSCs and CSS effectively retards LV remodeling and successfully improves LV performance.

In this study, readers would be highly interested in exploring the underlying mechanism of combined ADMSCs and CSS in alleviating LV remodeling and strengthening cardiac function in elderly patients with MI. We propose two fundamental findings that delineate the mechanisms underlying this successful treatment. First, 'reduction in WS force,' that is, after opening the chest wall, the CSS was patched on the LV IA, followed by firm sutures at 8 points and four suture lines crosstied over the CSS (Fig. 10), to constitute a 'restrictive chamberdilatation force,' resulting in retardation of LV dilatation and LV remodeling. Second, 'tissue engineering and regeneration,' that is, on day 180 after AMI induction, fibrosis fully occupied the IA (Fig. 7), suggesting myocardial death in the infarcted area, which was clearly identified in old MI animals. However, the histopathological findings identified that some 'islet-shape' survival myocardium cells were present inside the infarcted area of ADMSCs + CSS-treated animals. Additionally, the wall thickness significantly increased in animals treated with ADMSCs + CSS. These two findings highlight that 'tissue

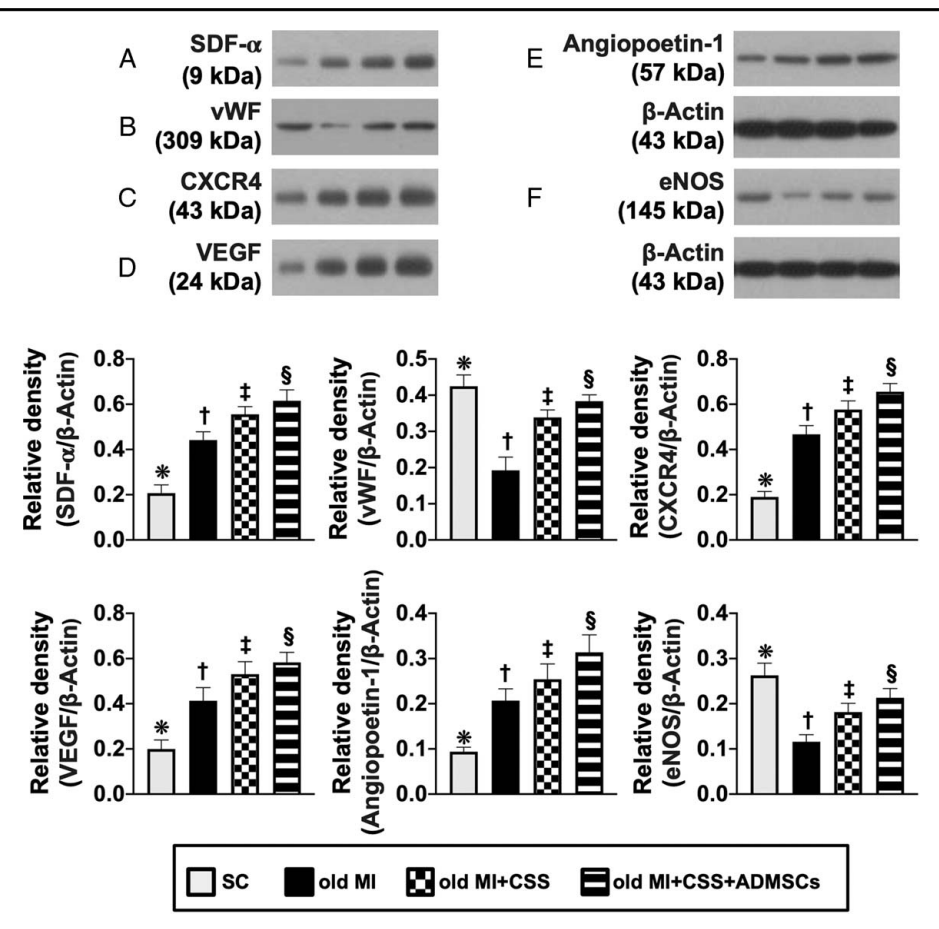


Figure 8. Protein levels of angiogenesis factors and integrity of endothelial cell biomarkers in the peri-infarcted area by 180th day after AMI induction. (A) Protein level of SDF-1 α , * versus other groups with different symbols (†, ‡, §), P < 0.0001. (B) Protein level of CXCR4, * versus other groups with different symbols (†, ‡, §), P < 0.0001. (C) Protein level of NEGF, * versus other groups with different symbols (†, ‡, §), P < 0.0001. (D) Protein level of angiopoetin-1, * versus other groups with different symbols (†, ‡, §), P < 0.0001. (E) Protein level of eNOS, * versus other groups with different symbols (†, ‡, §), P < 0.0001. (P) Protein level of eNOS, * versus other groups with different symbols (†, ‡, §) express significance (at 0.05 level).

engineering and regeneration' already occurred after ADMSCs + CSS treatment.

The upregulation of angiogenesis is crucial in restoring ischemiarelated organ dysfunction. In contrast, the upregulation of molecular-cellular perturbations, including inflammatory response, generation of oxidative stress, fibrosis, and apoptosis, including DNA-damage markers, correlate with worsening ischemia-related organ dysfunction^[9,15,19-23,26-28]. The essential findings in the current study were that, compared with old MI animals without treatment, the angiogenesis capacity (number of small vessels and protein levels of angiogenesis biomarkers) and anti-apoptotic gene expressions notably increased. In contrast, those of the molecular-cellular perturbations and gene expressions of inflammation, oxidative stress, and apoptosis mentioned above were remarkably repressed in ADMSCs + CSS-treated and further notably increased in SW-pretreated ADMSCs + CSS-treated animals. Our findings, in addition to corroborating the findings of previous reports [9,15,19-23,26-28], could, at least partly justify why LV remodeling was substantially suppressed and why LVEF was greatly retained in old MI animals after ADMSCs-CSS treatment.

Mitochondrial dysfunction and interruption of mitochondrial homeostasis play crucial roles in ischemic organs^[23,31]. A key finding in the current study was that compared with SC animals,

the mitochondrial damage marker was significantly increased. In contrast, the protein expression of complexes I–IV was significantly reduced in old MI animals. However, these variables were markedly reversed in ADMSCs + CSS-treated and further markedly reversed in SW-pretreated ADMSCs + CSS-treated animals. Our findings, in addition to strengthening those of previous reports^[23,31], explain why LV function was greatly preserved in old MI animals after acquiring SW-pretreated ADMSCs-CSS treatment.

Readers would be interested in the rationale for using mini-pigs for MI animal model studies and the translational aspects of this research. These animals have several physiological properties of humans^[26], including (1) similar body temperature and systolic and diastolic blood pressure; (2) almost identical heart rate and LV systolic and LV end-diastolic pressure; (3) same ratio of heart weight to body weight, ~1:10; (4) equal LV injection fraction; and (5) anatomical heart structures, giving >90% similarity of the coronary artery anatomy. In the near future, a large animal model will be used to facilitate applications in translational medicine. Additionally, our promising results and ethical methods may encourage cardiovascular surgeons to consider SW-pretreated ADMSCs seeded in CSS in the setting of coronary artery bypass surgery, particularly for those with incomplete revascularization

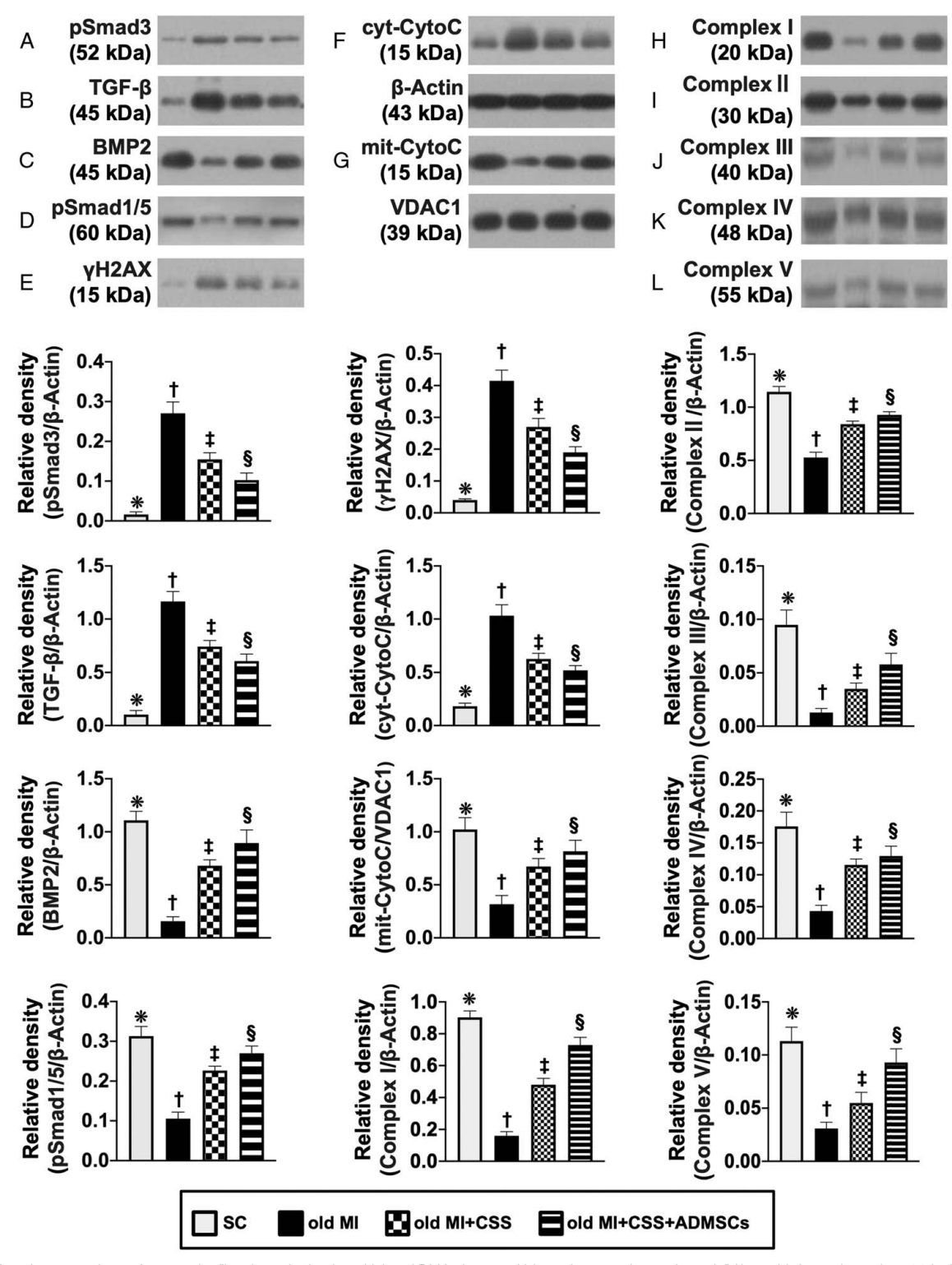


Figure 9. Protein expressions of apoptotic, fibrotic and mitochondrial and DNA-damaged biomarkers, and complexes I–IV in peri-infarcted area by 180th day after AMI induction. (A) Protein level of Smad3, * versus other groups with different symbols (†, ‡, §), P < 0.0001. (B) Protein level TGF-β, * versus other groups with different symbols (†, ‡, §), P < 0.0001. (C) Protein level of bone morphogenic protein (BMP)2, * versus other groups with different symbols (†, ‡, §), P < 0.0001. (D) Protein level of Smad1/5, * versus other groups with different symbols (†, ‡, §), P < 0.0001. (E) Protein level of γ -H2AX, * versus other groups with different symbols (†, ‡, §), P < 0.0001. (F) Protein level of cytosolic cytochrome C (cyt-CytoC), * versus other groups with different symbols (†, ‡, §), P < 0.0001. (G) Protein level of mitochondrial cytochrome C (mit-CytoC), * versus other groups with different symbols (†, ‡, §), P < 0.0001. (I) Protein level of complex II, * versus other groups with different symbols (†, ‡, §), P < 0.0001. (I) Protein level of complex II, * versus other groups with different symbols (†, ‡, §), P < 0.0001. (L) Protein level of complex II, * versus other groups with different symbols (†, ‡, §), P < 0.0001. (L) Protein level of complex II, * versus other groups with different symbols (†, ‡, §), P < 0.0001. (L) Protein level of complex V, * versus other groups with different symbols (†, ‡, §), P < 0.0001. (L) Protein level of complex V, * versus other groups with different symbols (†, ‡, §), P < 0.0001. (L) Protein level of complex V, * versus other groups with different symbols (†, ‡, §), P < 0.0001. (L) Protein level of complex V, * versus other groups with different symbols (†, ‡, §), P < 0.0001. (L) Protein level of complex V, * versus other groups with different symbols (†, ‡, §), P < 0.0001. (L) Protein level of complex V, * versus other groups with different symbols (†, ‡, §), P < 0.0001. (L) Protein level of complex V, * versus other groups with different

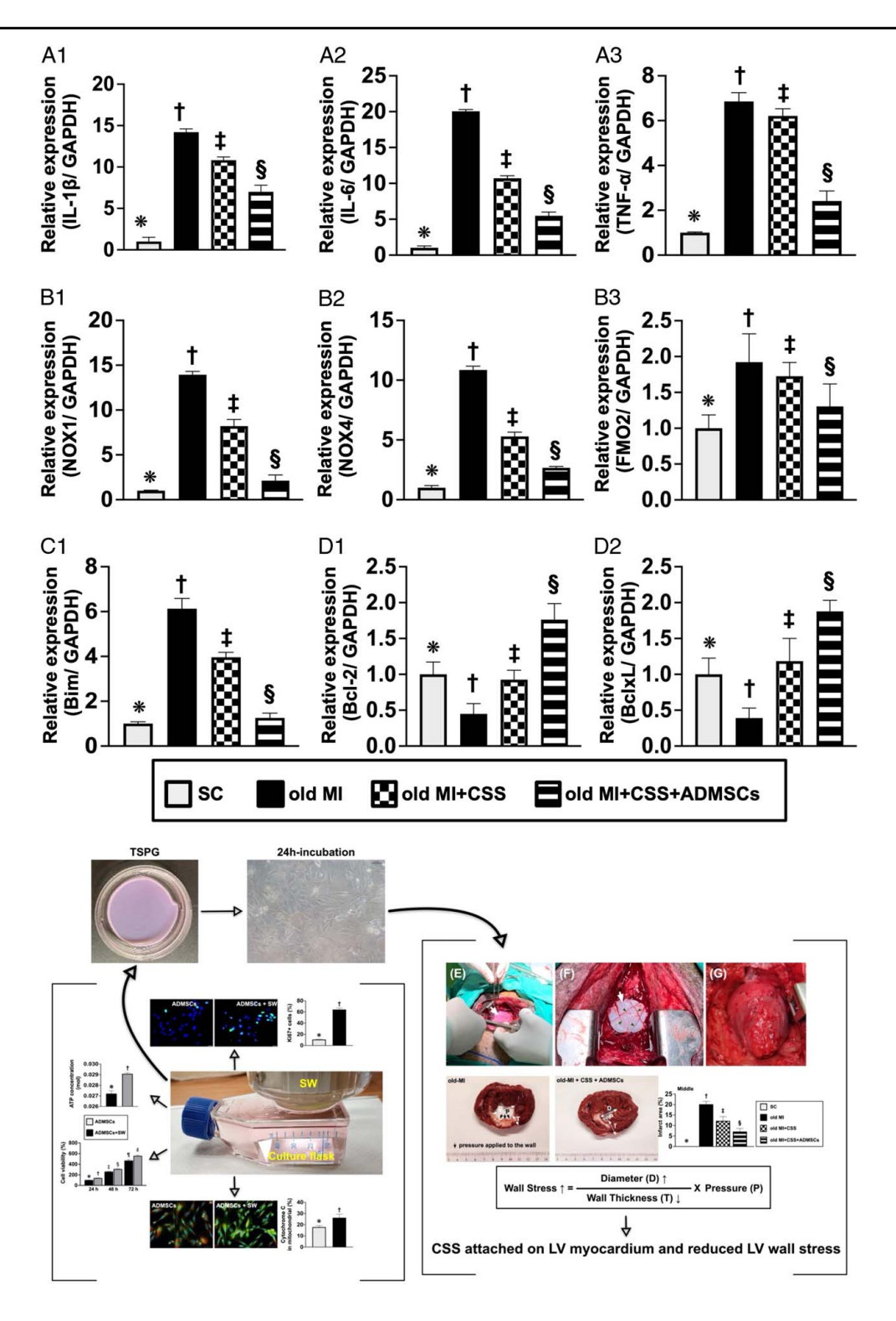


Figure 10. qPCR analyses of inflammation, oxidative stress, apoptosis, and anti-apoptosis in the peri-infarcted area by 180th day and proposed mechanism of SW-pretreated ADMSCs seeded in CSS patched on LV wall for attenuating LVWSF and improving heart function in MI pig. (A1) Relative gene expression of interleukin (IL)-1 β , * versus other groups with different symbols (†, ‡, §), P < 0.0001. (A2) Relative gene expression of IL-6, * versus other groups with different symbols (†, ‡, §), P < 0.0001. (B1) Relative gene expressions of NOX-1, * versus other groups with different symbols (†, ‡, §), P < 0.0001. (B2) Relative gene expression of NO-4, * versus other groups with different symbols (†, ‡, §), P < 0.0001. (B3) Relative gene expression of FMO2 (flavin-containing dimethylaniline monooxygenase 2), * versus other groups with different symbols (†, ‡, §), P < 0.0001. (C1) Relative gene expression of Bcl-2, * versus other groups with different symbols (†, ‡, §), P < 0.0001. (C2) Relative gene expression of Bcl-2, * versus other groups with different symbols (†, ‡, §), P < 0.0001. (D1) Relative gene

symbols (\uparrow, \uparrow, \S) , P < 0.0001. n = 5 for each group. ADMSCs, adipose-derived mesenchymal stem cells; CSS, cell-sheet scaffold; LV, left ventricular; LVWSF, LV wall stress force; MI, myocardial infarction; TSPG, temperature-sensitive plasticity gel; SW, shock wave. (E) Illustrating during suturing of SSC on LV wall. White arrows indicate the CSS with white color. (F) Illustrating the complete suture and the suture lines (green arrowheads) for firmly fixing the CSS on the LV-free wall can be clearly identified. (G) Demonstrating the gross anatomical morphology of the heart by the 180th day after IM induction. The CSS on the completely absorbed LV-free wall can be clearly identified.

owing to the coronary artery anatomy and distribution.

We did not determine whether ADMSCs seeded in CSS were superior to others for the following reasons. Currently, the two most popular methods for the administration of stem cell therapy for ischemic myocardium during cardiovascular surgery are direct implantation of stem cells into ischemic regions of the LV myocardium and cell-sheet scaffold patches on the LV-free wall. The first method has several disadvantages, including (1) direct implantation of stem cells into the myocardium containing even a small volume of the culture medium would damage the myocardium (by needle puncture and expanded volume), particularly when several sites of the ischemic myocardium should be injected with mixed cells + culture medium that contains some volume; and (2) after implantation, stem cells are always trapped at the implanted site and cannot migrate to remote areas. However, such an ischemic zone usually occurs in cases of inflammation, hypoxia, and oxidative stress, which can damage and kill implanted stem cells. However, the second method has several advantages: (1) cellsheet scaffold patches on the LV-free wall would not damage the myocardium; (2) the cells easily migrate into the LV myocardium from the cell sheet for differentiation and tissue regeneration; and (3) the cell sheet would provide basic requirements of nutrients that ensure cell survival in toxic environments.

Clinicians must always inquire whether the technology and results of the preclinical studies are ready and available for application in daily clinical practice. Considering that the present study was feasible and safe with attractive and promising results, we suggest applying ECSW and embedded ADMSCs + CSS into LV myocardium in cases of incomplete revascularization of coronary artery bypass grafting (CABG) surgery or in patients with myocardium ischemia and angina who are not candidates for CABG but refractory to medication, particularly when these technologies, treatment materials, and modalities are available without unethical issues.

Our study had some limitations. First, we could not measure the applied 'restrictive chamber-dilatation force' in the LV myocardium after CSS was patched on the LV infarcted area. Second, our study did not investigate the time points of ADMSCs-CSS treatment. Thus, whether the time interval of day 28 of treatment was most suitable to offer the greatest benefit for boosting the outcome in the old MI scenario remains unknown. Third, a group involving the direct implantation of ADMSCs into old MI animals was not included; hence, whether ADMSCs-CSS treatment was superior to ADMSCs treatment alone in improving LV performance or vice versa remains unknown. Fourth, despite extensive work, our data may only partially support the understanding of SW-supported ADMSCs-CSS treatment for improving LV function and inhibiting LV remodeling.

Conclusion

Our study showed that SW-pretreated ADMSCs-CSS offered great benefits in promoting LV performance and suppressing LV remodeling, mainly by counteracting Laplace's Law of LV WS.

Ethical approval

All animal experimental procedures were approved by the Institutional Animal Care and Use Committee at Kaohsiung Chang Gung Memorial Hospital, 123, Dapi Road, Niaosung, Kaohsiung 833401, Taiwan, ROC (Affidavit of Approval of Animal Use Protocol No. 2019031904) and performed in accordance with the Guide for the Care and Use of Laboratory Animals, 8th edition (NIH publication No. 85-23, National Academy Press, Washington, DC, USA, revised 2011).

Consent

Not applicable.

Source of funding

This study was supported by a program grant from Chang Gung Memorial Hospital, Chang Gung University (CRRPG8J0101, CRRPG8J0102, CRRPG8J0103, CMRPG8I0241). The funding body played no role in the design of the study and collection, analysis, and interpretation of data and in writing the manuscript.

Author contribution

J.-J.S., P.-H.S., and H.-K.Y.: conceptualization; J.-J.S., J.-N.Y., Y.-C.C., P.-H.S., C.-R.H., and Y.-C.L.: investigation; J.-J.S., C.-R.H., and P.-H.S.: methodology; J.-J.S.: funding acquisition; J.-J.S. and H.-K.Y.: supervision; J.-J.S. and H.-K.Y.: writing – original draft; J.-J.S., J.-Y.C., and H.-K.Y.: writing – review and editing. All authors read and approved the final manuscript in the last statement.

Conflicts of interest disclosure

The authors declare no conflicts of interest.

Research registration unique identifying number (UIN)

Not applicable.

Guarantor

Jiunn-Jye Sheu and Hon-Kan Yip.

Data availability statement

The datasets of the present study can be available from the corresponding author upon request.

Provenance and peer review

Guest Editor: Kandiah Raveendran; Theme: Shockwave treatment.

Acknowledgement

We would like to thank Editage (www.editage.com.tw) for editing the English language.

References

- [1] Nordlander R, Nyquist O. Mortality, arrhythmias and pump failure in acute myocardial infarction in relation to estimated infarct size. Acta Med Scand 1979:206:65–71.
- [2] Erlebacher JA, Weiss JL, Weisfeldt ML, et al. Early dilation of the infarcted segment in acute transmural myocardial infarction: role of infarct expansion in acute left ventricular enlargement. J Am Coll Cardiol 1984;4:201–8.
- [3] Pfeffer MA, Lamas GA, Vaughan DE, et al. Effect of captopril on progressive ventricular dilatation after anterior myocardial infarction. N Engl J Med 1988;319:80–6.
- [4] Pfeffer MA, Braunwald E, Moye LA, *et al.* Effect of captopril on mortality and morbidity in patients with left ventricular dysfunction after myocardial infarction. Results of the survival and ventricular enlargement trial. The SAVE Investigators. N Engl J Med 1992;327:669–77.
- [5] Mann DL. Mechanisms and models in heart failure: a combinatorial approach. Circulation 1999;100:999–1008.
- [6] Cohn JN, Ferrari R, Sharpe N. Cardiac remodeling--concepts and clinical implications: a consensus paper from an international forum on cardiac remodeling. Behalf of an International Forum on Cardiac Remodeling. J Am Coll Cardiol 2000;35:569–82.
- [7] Saku K, Kakino T, Arimura T, et al. Total mechanical unloading minimizes metabolic demand of left ventricle and dramatically reduces infarct size in myocardial infarction. PLoS One 2016;11:e0152911.
- [8] Kapur NK, Reyelt L, Swain L, et al. Mechanical left ventricular unloading to reduce infarct size during acute myocardial infarction: insight from preclinical and clinical studies. J Cardiovasc Transl Res 2019;12:87–94.
- [9] Lin KC, Yip HK, Shao PL, et al. Combination of adipose-derived mesenchymal stem cells (ADMSC) and ADMSC-derived exosomes for protecting kidney from acute ischemia-reperfusion injury. Int J Cardiol 2016;216:173–85.
- [10] Chang CL, Sung PH, Chen KH, et al. Adipose-derived mesenchymal stem cell-derived exosomes alleviate overwhelming systemic inflammatory reaction and organ damage and improve outcome in rat sepsis syndrome. Am J Transl Res 2018;10:1053–70.
- [11] Chang CL, Chen HH, Chen KH, et al. Adipose-derived mesenchymal stem cell-derived exosomes markedly protected the brain against sepsis syndrome induced injury in rat. Am J Transl Res 2019;11:3955–71.
- [12] Yip HK, Fang WF, Li YC, et al. Human umbilical cord-derived mesenchymal stem cells for acute respiratory distress syndrome. Crit Care Med 2020:48:e391–9.
- [13] Chen YT, Chuang FC, Yang CC, et al. Combined melatonin-adipose derived mesenchymal stem cells therapy effectively protected the testis from testicular torsion-induced ischemia-reperfusion injury. Stem Cell Res Ther 2021;12:370.
- [14] Wu HJ, Yiu WH, Wong DWL, *et al.* Human induced pluripotent stem cell-derived mesenchymal stem cells prevent adriamycin nephropathy in mice. Oncotarget 2017;8:103640–56.
- [15] Ko SF, Chen YT, Wallace CG, et al. Inducible pluripotent stem cellderived mesenchymal stem cell therapy effectively protected kidney

- from acute ischemia-reperfusion injury. Am J Transl Res 2018;10: 3053-67.
- [16] Soontararak S, Chow L, Johnson V, et al. Mesenchymal stem cells (MSC) derived from induced pluripotent stem cells (iPSC) equivalent to adiposederived MSC in promoting intestinal healing and microbiome normalization in mouse inflammatory bowel disease model. Stem Cells Transl Med 2018;7:456–67.
- [17] Simpson D, Liu H, Fan TH, et al. A tissue engineering approach to progenitor cell delivery results in significant cell engraftment and improved myocardial remodeling. Stem Cells 2007;25:2350–7.
- [18] Simpson DL, Dudley SC Jr. Modulation of human mesenchymal stem cell function in a three-dimensional matrix promotes attenuation of adverse remodelling after myocardial infarction. J Tissue Eng Regen Med 2013;7: 192–202.
- [19] Sun CK, Zhen YY, Leu S, et al. Direct implantation versus platelet-rich fibrin-embedded adipose-derived mesenchymal stem cells in treating rat acute myocardial infarction. Int J Cardiol 2014;173:410–23.
- [20] Fu M, Sun CK, Lin YC, et al. Extracorporeal shock wave therapy reverses ischemia-related left ventricular dysfunction and remodeling: molecularcellular and functional assessment. PLoS One 2011;6:e24342.
- [21] Sheu JJ, Ali HEE, Cheng BC, et al. Extracorporeal shock wave treatment attenuated left ventricular dysfunction and remodeling in mini-pig with cardiorenal syndrome. Oncotarget 2017;8:54747–63.
- [22] Yin TC, Wu RW, Sheu JJ, et al. Combined therapy with extracorporeal shock wave and adipose-derived mesenchymal stem cells remarkably improved acute ischemia-reperfusion injury of quadriceps muscle. Oxid Med Cell Longev 2018;2018:6012636.
- [23] Sung PH, Lee MS, Chai HT, et al. Extracorporeal shock wave enhanced exogenous mitochondria into adipose-derived mesenchymal stem cells and further preserved heart function in rat dilated cardiomyopathy. Biomedicines 2021;9:1362.
- [24] Kilkenny C, Browne WJ, Cuthill IC, et al. Improving bioscience research reporting: the ARRIVE guidelines for reporting animal research. PLoS Biol 2010;8:e1000412.
- [25] Chen W, Hou CH, Chen YL, et al. Safety and efficacy of intracoronary artery administration of human bone marrow-derived mesenchymal stem cells in STEMI of Lee-Sung pigs-a preclinical study for supporting the feasibility of the OmniMSC-AMI phase I clinical trial. Front Cardiovasc Med 2023;10:1153428.
- [26] Leu S, Sun CK, Sheu JJ, et al. Autologous bone marrow cell implantation attenuates left ventricular remodeling and improves heart function in porcine myocardial infarction: an echocardiographic, sixmonth angiographic, and molecular-cellular study. Int J Cardiol 2011; 150:156–68.
- [27] Sheu JJ, Lee FY, Yuen CM, *et al.* Combined therapy with shock wave and autologous bone marrow-derived mesenchymal stem cells alleviates left ventricular dysfunction and remodeling through inhibiting inflammatory stimuli, oxidative stress & enhancing angiogenesis in a swine myocardial infarction model. Int J Cardiol 2015;193:69–83.
- [28] Sun CK, Shao PL, Wang CJ, et al. Study of vascular injuries using endothelial denudation model and the therapeutic application of shock wave: a review. Am J Transl Res 2011;3:259–68.
- [29] Pfau D, Thorn SL, Zhang J, *et al.* Angiotensin receptor neprilysin inhibitor attenuates myocardial remodeling and improves infarct perfusion in experimental heart failure. Sci Rep 2019;9:5791.
- [30] Hwang SY, Kim SH, Uhm IA, et al. Prognostic implications for patients after myocardial infarction: an integrative literature review and in-depth interviews with patients and experts. BMC Cardiovasc Disord 2022;22:348.
- [31] Yeh JN, Yue Y, Chu YC, et al. Entresto protected the cardiomyocytes and preserved heart function in cardiorenal syndrome rat fed with high-protein diet through regulating the oxidative stress and Mfn2-mediated mitochondrial functional integrity. Biomed Pharmacother 2021;144: 112244.